Operation of Lorentz-Force MEMS Magnetometers With a Frequency Offset Between Driving Current and Mechanical Resonance

Giacomo Langfelder[1] and Alessandro Tocchio[2]

[1]Politecnico di Milano, Dipartimento di Elettronica, Informazione e Bioingegneria, 20133 Milano, Italy
[2]ST Microelectronics, AMS Division, Cornaredo, Milano, Italy

I. Introduction

THE integration of a 3-axis accelerometer, a 3-axis gyroscope and a 3-axis magnetometer in a single-chip is the present focus of research in different fields of application [1], [2]. Such a combination of sensors—a so called 9-axis inertial measurement unit (or IMU)—would allow for instance precise motion reconstruction even in absence of GPS signals in dead reckoning systems.

At the state of the art, there are examples of 6-axis IMUs [3], [4] built in a single chip using microelectromechanical system (MEMS) technologies. 3-axis magnetometers based on anisotropic magnetoresistance (AMR) [5], [6], magnetic tunnel junction (MTJ) [7] or Hall-effect [8], [9] are instead still more popular than their MEMS counterpart, either as stand-alone devices or within 9-axis IMUs [9].

Several examples of MEMS magnetometers were proposed in the literature; most of them are based on the Lorentz-force principle (motion is excited by a current injected at resonance) and use capacitive readout [2], [10]–[13]. It has been shown that the performance of all of these devices is more or less comparable in terms of resolution per unit bandwidth and unit driving current (e.g., in $\mathrm{nT} \bullet \mathrm{mA}/\sqrt{\mathrm{Hz}}$) [14]. This parameter is taken as a figure of merit (FOM) in this paper as it can be used (in addition to linear full-scale-range, FSR) to compare devices built in the different technologies mentioned above.

Intrinsic issues of resonant Lorentz-force devices studied so far in the literature can be summarized as follows:

— there is a marked trade-off between the gain-factor (here defined as the capacitance variation per unit magnetic flux density) and the maximum sensing bandwidth, which shows an opposite dependence on the quality factor;
— the gain-factor does not improve with the number of sensing cells when using parallel-plate capacitive readout [1];
— other issues, later detailed in Section II, are related to the implementation of the driving oscillator circuit, required to inject a stable ac current exactly at the resonance frequency.

In this paper it is proposed the operation of Lorentz-force magnetometers with a frequency offset Δf between the driving frequency f_d of the injected Lorentz current and the mechanical resonance frequency f_s (see Fig. 1). This approach is inspired by the operation of gyroscopes with a frequency mismatch between the driving and sensing modes [15], [16], and leads to the following considerations:

— the maximum sensing bandwidth is extended to roughly 1/3 of the frequency offset Δf;
— the gain-factor is not as large as for resonant sensing, but it is still e.g., more than 30 times the dc gain;
— the operation occurs around f_d, in a relatively flat gain-factor region, if compared to operation around the peak of a high Q-factor transfer function (see again Fig. 1). This makes the system significantly immune to small variations $\sigma_{\Delta \mathrm{f}}$ in the frequency offset Δf, caused by fabrication spreads;
— for the same reason as above, i.e. the lower sensitivity to process variance, a single driving current at a frequency f_d can be used to drive a three-axis device. This immediately leads to a save in current consumption by a factor three.

The paper reviews and compares in Section II the theory of operation of Lorentz-force magnetometers, both operated at resonance and operated with the proposed frequency split. Section III describes and characterizes a MEMS magnetometer in terms of gain-factor when operated with a frequency offset. Section IV extends the discussion to noise and compares the obtainable FOM of such Lorentz-force magnetometers with existing Hall, MTJ and AMR devices.

Manuscript received July 17, 2013; revised September 01, 2013; accepted September 07, 2013. Date of publication September 11, 2013; date of current version December 23, 2013. Corresponding author: G. Langfelder (e-mail: langfelder@elet.polimi.it).

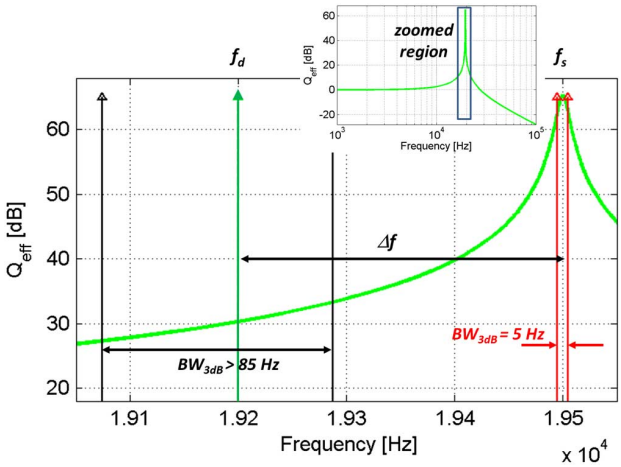

Fig. 1 Force-to-displacement transfer function for a MEMS device. If the device is excited with a frequency mismatch (e.g., $\Delta f = 300$ Hz) from the resonance (e.g., $f_s = 19.5$ kHz), the gain decreases (e.g., from 65 dB to 31 dB) but the ± 3 dB bandwidth is extended (e.g., from 5 Hz to more than 85 Hz).

II. Theory of Operation

The schematic representation of a z-axis Lorentz-force magnetometer is shown in Fig. 2. Suitable sustaining springs, anchored to the substrate on one side, hold a central shuttle that forms with fixed electrodes (stators) a set of two differential parallel-plate capacitors, each with a nominal rest value C_0, formed by N cells of facing area A and nominal gap g in between the plates. An ac current $i(t)$ flowing through the springs generates, in presence of a component B of the magnetic flux density along the z-axis, a Lorentz force distributed on the length L whose intensity is given by

$$F_L(t) = i(t) \cdot B \cdot L. \tag{1}$$

The force determines a displacement x in the horizontal direction, which—in small displacement approximation—can be read as a differential capacitance change ΔC (with ε_0 assumed as the permittivity of vacuum) [17]:

$$\Delta C = 2C_0 \frac{x}{g} = \frac{2N\varepsilon_0 A}{g^2} x. \tag{2}$$

A. Operation at Resonance

If the device is operated with the ac current at the mechanical resonance frequency f_s of the first mode (corresponding to a translation in the x-direction), the force-to-displacement transfer function is amplified by the quality factor Q with respect to the dc value stiffness k and therefore

$$x = \frac{Q}{2k} i \cdot B \cdot L \tag{3}$$

(the factor 2 at the denominator accounts for the distributed force across the springs). If operation is in the molecule-flow regime [25] (as often occurs for MEMS packaged in the 0.1 to 10 mbar pressure range) the gain-factor can be written as [2]:

$$\frac{\Delta C}{\Delta B} = \frac{2N\varepsilon_0 A}{g^2} \frac{Q}{2k} i \cdot L = \frac{\varepsilon_0 \cdot L \cdot i}{4\pi f_s \cdot g^2 \cdot b_{\text{area}}} \tag{4}$$

where the following relations have been used:

$$Q = \frac{2\pi f_s \cdot m}{b}, \quad f_s = \frac{1}{2\pi}\sqrt{\frac{k}{m}}, \quad b = 2b_{\text{area}} N \cdot A. \tag{5}$$

In the formulas above, b is the damping coefficient: it is known that this parameter linearly depends on the facing length of the parallel plates [18]. If we assume the suspended mass height as a fixed process parameter, b can be written in terms of its value per unit area b_{area}; finally m is the effective device mass. The intrinsic (i.e., related to the device only) signal-to-noise ratio for operation at resonance can be conveniently written in terms of displacements starting from the thermo-mechanical noise ($S_{F,n}$, in units of N^2/Hz; T is the absolute temperature, k_b the Boltzmann constant):

$$\begin{aligned} SNR_{res} &= \frac{x}{\sqrt{S_{F,n} \cdot \frac{Q^2}{k^2} \cdot BW_{-3dB}}} \\ &= \frac{\frac{Q}{2k} i \cdot B \cdot L}{\sqrt{4k_b T b \cdot \frac{Q^2}{k^2} \cdot BW_{-3dB}}}. \end{aligned} \tag{6}$$

The readout bandwidth BW_{-3dB} is assumed as the maximum achievable one determined by the quality factor ($BW_{-3dB} = f_s/2Q$). By setting the SNR equal to 1, the minimum detectable magnetic flux density variation can be derived:

$$B_{\min,res} = \frac{8 \cdot BW_{-3dB}}{i \cdot L} \sqrt{\pi k_b T \cdot m} = \frac{4 \cdot f_s}{i \cdot L \cdot Q} \sqrt{\pi k_b T \cdot m}. \tag{7}$$

A large bandwidth directly implies a low quality factor and a worse resolution. Once the area (thus the length), the power dissipation (thus the current) and the bandwidth are fixed by the application specifications, it is difficult to improve the sensitivity, which from (4) is independent on the number of sensing cells N. Some comments needs also to be made about the circuit needed to inject the current through the springs at the resonance frequency:

- on one side, an oscillator circuit whose loop does not include the mechanical resonator of the magnetometer (open-loop current driving) is not attainable because the resonance frequency and quality factor of the magnetometers are affected by process variance, temperature and aging. These would lead, as for gyroscopes [15], to unacceptable gain-factor changes, both from part to part and on each device under different environmental conditions;
- on the other side, it is also difficult to implement a driving circuit through a closed-loop oscillator at resonance (i.e., an oscillator which includes the device as the resonating element [19]), because the motional current and thus the loop-gain of the oscillator are themselves dependent on the intensity of the magnetic flux density B along the sensing direction;
- in a three-axial implementation with three different sensing structures it would be impossible to drive them with the same current source at a nominal frequency f_s because, due to process variance, the three MEMS would typically show different peak frequencies even when designed to be identical (all the considerations above were

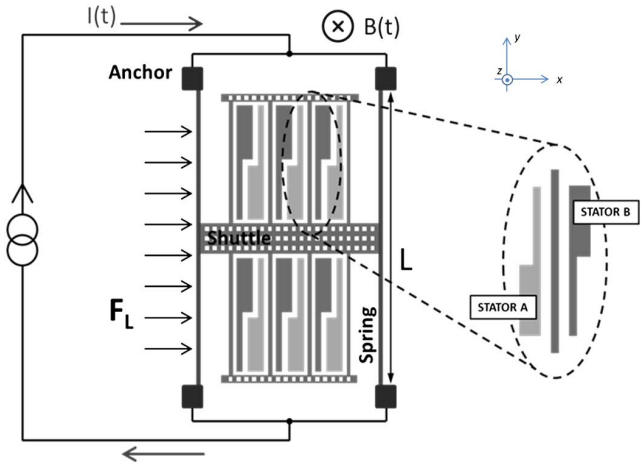

Fig. 2 Schematic representation of a Lorentz-force MEMS magnetometer. An ac current is injected through the springs; in presence of a magnetic flux density B in the out-of-plane direction, a force determines an ac displacement whose amplitude is proportional to B. The displacement can be read out through the differential capacitive change between the moving shuttle plates and the fixed stators.

given for a z-axis device but the same discussion holds for the x- or y-axis [13]).

B. Operation With a Frequency Split

The method here proposed to extend the bandwidth and to solve the above discussed issues is to operate with an offset between the resonance frequency f_s of the magnetometer and the frequency f_d of the driven current. In this situation, an open-loop drive current at f_d can be derived either from an electronic oscillator, or from an auxiliary MEMS-resonator-based oscillator. The latter case is preferable as the variance $\sigma_{\Delta \mathrm{f}}$ in the frequency split Δf from part to part and its changes with temperature would be strongly reduced, as the resonator and the magnetometer can be designed in such a way that their frequencies are affected in a similar way by process and temperature changes [15].

The Laplace transfer function between the Lorentz force and the magnetometer displacement in the general case reads:

$$\frac{x(s)}{F_L(s)} = \frac{1}{m} \cdot \frac{1}{s^2 + \frac{b}{m}s + \frac{k}{m}}. \tag{8}$$

Its modulus for a Lorentz-force frequency f_d, excited by the current properly pumped with an offset $\Delta f = f_s - f_d$, can be derived by setting $s = j\omega_d$, $\omega_d = 2\pi f_d$ and $\omega_s = 2\pi f_s$:

$$\left|\frac{x\,(j\omega_d)}{F_L\,(j\omega_d)}\right| = \left|\frac{1}{m} \cdot \frac{1}{\left(-{\omega_d}^2 + j\frac{\omega_s}{Q}\omega_d + {\omega_s}^2\right)}\right| = \frac{1}{m} \cdot \frac{1}{\sqrt{\left({\omega_s}^2 - {\omega_d}^2\right)^2 + \left(\frac{\omega_s}{Q}\omega_d\right)^2}}. \tag{9}$$

In case *(i)* $Q \gg 1$, *(ii)* the frequency offset Δf is much lower than f_s and *(iii)* Δf is also much larger than the mechanical bandwidth $f_s/2Q$ (e.g., $f_s \sim 20$ kHz, $Q \sim 1000$ and $\Delta f \sim 300$), the transfer function can be reasonably approximated as almost flat around the operating point. Equation (9) indeed simplifies into

$$\left|\frac{x(j\omega_d)}{F_L(j\omega_d)}\right| = \frac{1}{m} \cdot \frac{1}{\sqrt{{\omega_s}^4 + {\omega_d}^4 - 2{\omega_s}^2{\omega_d}^2 + \cancel{\left(\frac{\omega_s}{Q}\omega_d\right)^2}}} = \sim \frac{1}{m} \cdot \frac{1}{{\omega_s}^2 - (\omega_s - \Delta\omega)^2} \sim \frac{1}{m} \cdot \frac{1}{2\omega_s\Delta\omega - \cancel{\Delta\omega^2}} = \frac{1}{k}\frac{\omega_s}{2\Delta\omega} = \frac{1}{k}Q_{eff} \tag{10}$$

where Q_{eff} represents an *effective* quality factor, i.e. the residual amplification obtained with an offset Δf from the resonance frequency f_s. One can therefore write the SNR as

$$\frac{SNR_{unm} = \frac{Q_{eff}}{2k} i \cdot B \cdot L}{\sqrt{4k_bTb \cdot \frac{{Q_{eff}}^2}{k^2} \cdot BW}} \tag{11}$$

where BW represents an electronic filter of a width within the ± 3 dB values indicated in Fig. 1 (one can think to it as applied after the demodulation at f_d). The minimum detectable signal depends on BW and on the damping coefficient:

$$B_{\min,unm} = \frac{4}{i \cdot L}\sqrt{k_bT \cdot b \cdot BW}. \tag{12}$$

Comparing (6) and (11) one can note that the expressions are similar: if the comparison is done for the same bandwidth, setting $BW = BW_{-3db}$, it turns out that the system with the largest SNR is simply the one with the lowest value for b. It therefore turns out that the SNR improves with a lower damping coefficient b, which is not surprising. The important point is that, in case of unmatched frequencies, b can be reduced (by acting on the geometry or on the pressure) with no impact on the bandwidth BW, which is defined by the electronics, whereas in case of matched frequencies b cannot be arbitrarily changed without impacts on BW_{-3db}.

From another point of view, in case of unmatched operation the bandwidth can be extended up to a relevant fraction of the frequency offset, while keeping a good intrinsic SNR if b is properly reduced. Care needs to be taken to electronically filter the resonant peak [15].

As a numerical example, a device with a quality factor of 1800 resonating around a 20 kHz frequency would have a bandwidth of 5 Hz only. The same device with an offset of 300 Hz can reach a ± 3 dB bandwidth of about 100 Hz, orders of magnitude higher than for frequency match.

It should be noted here that the SNR and minimum measurable flux density refer to the device noise only: further discussion on the electronic noise will be given in Section IV.

Finally, the larger is the frequency offset, the higher becomes the tolerance to process variation. As a consequence:

- the issue of the implementation of the driving oscillator can be potentially solved: indeed it is not problematic if the oscillator frequency does not match exactly the intended f_d;
- 3-axis devices with the same nominal resonant frequency f_s can be potentially driven with a single current at f_d, provided that their effective frequency, nominally identical, turns out to be different (e.g., due to process variations or deviations from numerical simulations) by an amount which is much lower than Δf. Electrostatic frequency tuning or a simple gain calibration may help in accommodating this requirement.

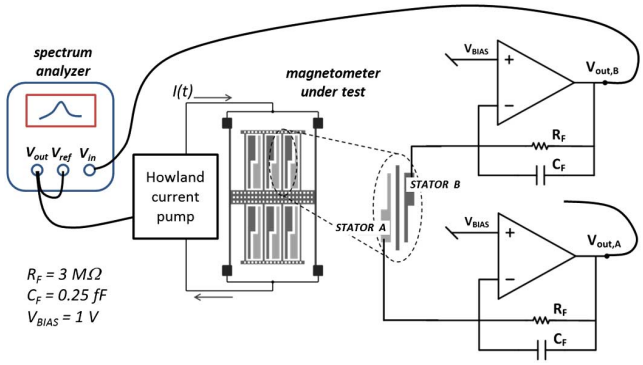

Fig. 3 Setup for the measurement of the gain-factor at different mismatches: an ac current (generated by a Howland current pump driven by the spectrum analyzer) is swept through the magnetometer at different frequencies. Single-ended capacitance changes are measured through a pair of transimpedance stages, one at a time (in the example, $V_{out,B}$ is being read).

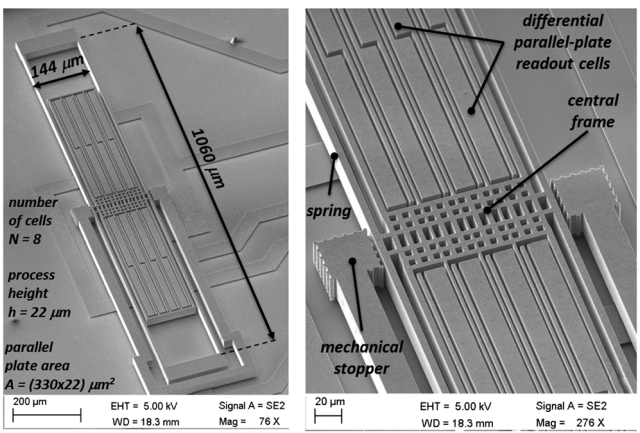

Fig. 4 SEM picture of the device used for the tests. The gap between plates at rest is nominally $g = 2.1$ μA and the overall stiffness is $k = 14$ N/m.

III. Experimental Results

In order to test the gain-factor of a device with a frequency offset between the drive current and the resonance peak, the setup shown in Fig. 3 was used. A Lorentz-force magnetometer, later described, is excited through a current whose frequency is swept through a spectrum analyzer. The differential capacitance variation is measured through a pair of discrete-component transimpedance amplifiers (TIA) with a 3 MΩ feedback resistance. Measurements are repeated under three different magnetic flux densities, generated through permanent magnets whose relative distance can be carefully changed with a sub-mm precision. In order to avoid interference from other fields, measurements are done at relatively large flux densities ($B > 1$ mT) with a relatively low driving current peak amplitude ($|i(t)| \sim 300$ μA). A setup calibration for B was preliminary performed through an Asahi Kasei reference Hall-type magnetometer [20].

The MEMS magnetometer used for the tests is built through the ST Microelectronics ThELMA (Thick Epitaxial Layer for Microactuators and Accelerometers) process. A scanning electron microscope (SEM) picture of the device and the relevant dimensions are reported in Fig. 4. The nominal resonance frequency is set around 20 kHz by design, in order to avoid disturbance from acoustic waves, as typically done for other consumer devices operated at resonance [21].

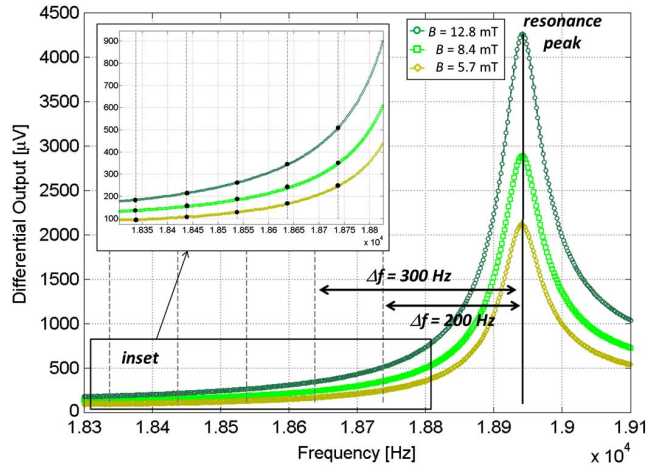

Fig. 5 Device experimental response under different magnetic flux densities. The inset shows the curves around splits Δf in the range of 200-600 Hz.

Fig. 5 reports the measurement results, with the driving current frequency f_d on the x-axis and the differential output of the two TIAs on the y-axis. The resonance peak occurs at 18.94 kHz at a voltage $V_{\mathrm{BIAS}} = 1$ V on the stators (applied through the virtual ground of the TIA). The peak sensitivity (at resonance) turns out to be about 0.3 mV/mT, with a quality factor around 360, in good agreement with theoretical predictions of (4). The corresponding bandwidth is easily found to be $BW_{-3db} = 26$ Hz. The product of the gain-factor and the bandwidth is therefore 7.8 Hz · mV/mT. The inset shows a zoom of the responses at frequency offsets Δf from 200 Hz to 600 Hz with respect to the resonance peak at f_s.

Fig. 6a deepens the results of Fig. 5 showing the output voltage, now as a function of the flux density B, parametrically reporting curves with different Δf. The constancy of the $\frac{\Delta C}{\Delta B} \cdot \Delta f$ product can be appreciated in Fig. 6b where the dashed curve represents the theoretical function at 7.8 Hz mV/mT and the markers are the experimental points.

The noise performance is in the current setup limited by the Johnson noise of the feedback resistances R of the TIA stages, integrated on the readout bandwidth of the spectrum analyzer $BW_{SA} \sim 30$ Hz (it was set similar to BW_{-3db}):

$$\sigma_{n,v}^2 = \sqrt{4k_bTR \cdot BW_{SA}}$$
$$\Delta B_{\min} = \frac{\sqrt{\sigma_{n,v}^2}}{0.3\frac{mV}{mT}} = 4.1\,\mu T_{rms} \qquad (13)$$

It was therefore not possible to verify within this work the intrinsic minimum measurable field, which (12) predicts to be lower than the value found from (13). Some considerations on the required noise performance for the readout electronics will be thus deepened in the next section.

IV. Discussion, Perspectives and Conclusion

The analysis and results shown in the previous sections will be now applied to the case of consumer-grade applications (navigation, heading, electronic compass…), for which typical requirements for the next years, regardless of the technology used for the implementation (AMR, MTJ, Hall-effect, MEMS), are summarized in Table I.

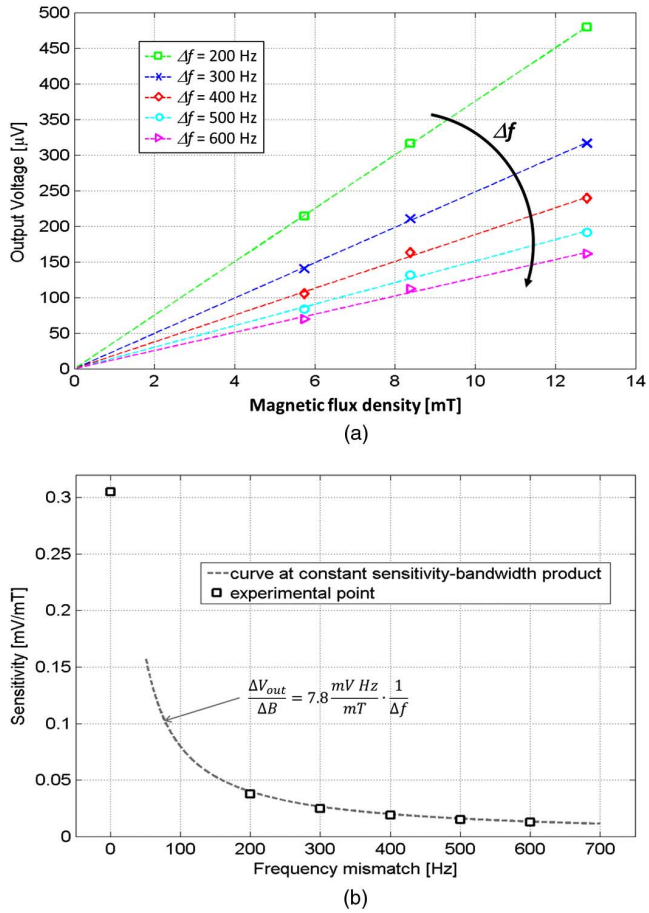

Fig. 6 (a) output voltage as a function of the input field and (b) obtained sensitivity at different frequency splits.

TABLE I
PARAMETERS FOR CONSUMER GRADE MAGNETOMETERS

Parameter	Target value
Maximum Full Scale Range	± 2.4 mT
Maximum Non-Linearity	± 1.5 %
Minimum field r.m.s.	500 nT
Bandwidth	50 Hz
Temperature range	-40 °C to +85 °C
Power consumption	1 mW for 3-axis

For comparison, some parameters and the figure of merit (FOM) defined as the resolution per unit current consumption of different state-of-the-art devices is reported in Table II along with the corresponding full-scale (FSR).

A. Minimum Field and Corresponding Capacitance Change

The minimum detectable magnetic flux density to guarantee a precision in heading of approximately 1° is around 500 nT [10]. Using the device presented in Section II, the minimum measurable magnetic flux density when operating at resonance with a low-noise electronics is, from (7)

$$B_{\min,res} = \frac{4 \cdot f_s}{i \cdot L \cdot Q} \sqrt{\pi k_b T \cdot m} = 2.4\,\mu T \qquad (14)$$

corresponding to a maximum bandwidth of $BW_{-3db} \sim 26$ Hz ($Q = 360$ at a pressure of 1 mbar). Neither the resolution nor the bandwidth are within the specifications of Table I. Lowering the pressure to improve the damping coefficient would have a negative effect on the bandwidth. Taking into account that for a tri-axis device three times the current i is needed, the FOM for this mode of operation is around $420\ \mu\text{T} \cdot \mu\text{A}/\sqrt{\text{Hz}}$.

On the other side, if we assume to operate the same device with a frequency split of 300 Hz, an electronic filtering bandwidth (e.g., applied after the demodulation) of 50 Hz (to match the value in Table I) and a low pressure obtainable with an industrial process using getter materials, ~ 0.05 mbar ($Q \sim 7200$), the measurable magnetic flux density from (12) is

$$B_{\min,unm} = \frac{4}{i \cdot L} \sqrt{k_b T \cdot b \cdot BW} = 0.7\,\mu T \qquad (15)$$

a factor 3.5 better than for resonant operation and close to the requirements of Table I. The correspding FOM with a single current for a 3-axis system turns out to be in the order of $\sim 29\ \mu\text{T} \cdot \mu\text{A}/\sqrt{\text{Hz}}$.

B. Further Improvements

Using the parameters above, the capacitance change corresponding to the minimum flux density to be detected is

$$\Delta C = \frac{2N\varepsilon_0 A}{g^2} \frac{Q_{eff}}{2k} i \cdot L \cdot B_{\min,unm} = 0.06\ aF. \qquad (16)$$

The derived requirement for an electronics, e.g., with a 3x-lower-noise on the full bandwidth BW, becomes $2.8\ \text{zF}/\sqrt{\text{Hz}}$.

Even if sub-$\text{zF}/\sqrt{\text{Hz}}$ resolution measurements have been demonstrated in the literature at relatively low currents [22], [23], to relieve the requirements on the readout electronics it would be good to increase the capacitance change corresponding to the minimum field.

A technique already proposed in the literature that goes in this direction is the use of multiple paths that allow the same current to re-circulate several times in each device [11]. Metal strips deposited and electrically isolated on top of the micro-machined material form these paths. With N_p multiple paths, this approach directly implies an output signal larger by the same factor. The FOM is N_p times lower and the capacitance change for the same flux density is N_p times larger. For example, with $N_p = 10$ as in the referenced paper, one gets for the flux density required by the specifications of Table I:

$$\Delta C = \frac{2N\varepsilon_0 A}{g^2} \frac{Q_{eff}}{2k} i \cdot N_p \cdot L \cdot 0.5\,\mu T = 0.43\ aF \qquad (17)$$

and the corresponding requirement for the electronic is $20\ \text{zF}/\sqrt{\text{Hz}}$. Such a capacitance variation can be readout with a relatively low-noise, low-power electronics (see, e.g., [24]) so that the noise contributions from the electronics can be at first order neglected. Similarly, the electronics consumption can be thought as a fraction of the one dissipated in the device.

C. Linearity and Full-Scale Range

Concerning the full scale range, as the Lorentz force is linear with B, main limitations can arise in the parallel-plate readout. However as reported in [14], for small displacements (with respect to the capacitive gap g) and using a differential configuration, the obtainable linear full-scale-range is far larger than what allowed by other technologies which have (e.g., in the case of

TABLE II
FIGURE OF MERIT FOR DIFFERENT DEVICES

Device	±FSR [mT]	Noise [μT]	Band** [Hz]	Current [μA]	FOM [μT·μA/√Hz]
STM LIS3MDL	1.6	0.4	40	270	17.1
Bosch BMM150	1.3	0.3	5	170	22.8
Freescale MAG3110	1	0.3	0.5	17	7.5
Asahi Kasei AK8975	1.2	0.25	4	350	43.7
Honeywell HMC1181	0.8	0.2	3.2	100	23.1
Lorentz (at resonance)*	> 2	2.4	26	900***	423.6
Lorentz (with offset)*	> 2	0.7	50	300	29.6
Lorentz (offset, 10 multipaths)*	> 2	0.07	50	300	3.0

* electronic noise, consumption assumed negligible fraction of device noise, consumption

** when output data rate (ODR) is given in the datasheets, the band is taken as $1/2$ ODR

*** three times the current of a single-axis device

AMR devices) intrinsic nonlinearity in the operating principle. In the end the FSR specified by Table I is not seen as an issue for MEMS magnetometers.

Looking finally at Table II, one can therefore conclude that Lorentz-force devices, which have been for a long time under scientific interest, can be very competitive with state-of-the-art and future products when operated with the proposed frequency offset technique, and can even go beyond the state-of-the-art by combining this approach with a multiple-path design, if allowed by the technology. The proposed approach can be exploited by other already-existing capacitive devices, e.g., [10]–[13], [26] and by Lorentz force magnetometers based on other readout techniques as well [27], [28]. The proposed approach is also more immune to temperature changes than operation at resonance, as temperature changes—which determine variations in the quality factor—do not significantly affect the gain-factor (as shown in 10).

Future work by the authors will include the design of tri-axis magnetometers optimized for operation with frequency offset, and corresponding integrated driving and sensing circuits for low-noise, low-power operation.

REFERENCES

[1] C. M. N. Brigante, N. Abbate, A. Basile, A. C. Faulisi, and S. Sessa, "Towards miniaturization of a MEMS-based wearable motion capture system," *IEEE Trans. Ind. Electron.*, vol. 58, no. 8, pp. 3234–3241, Aug. 2011.

[2] G. Langfelder, C. Buffa, A. Frangi, A. Tocchio, E. Lasalandra, and A. Longoni, "Z-axis magnetometers for MEMS inertial measurement units using an industrial process," *IEEE Trans. Ind. Electron.*, vol. 60, no. 9, Sep. 2013.

[3] *LSM330DLC: 3D Accelerometer + 3D Gyroscope Technical Datasheet*. Geneva, Switzerland: STMicroelectronics, 2011 [Online]. Available: http://www.st.com.

[4] *MPU-6100/MPU-6150: 3D Accelerometer + 3D Gyroscope Product Specification*. Sunnyvale, CA: InvenSense, 2012 [Online]. Available: http://invensense.com/mems/gyro/documents/PSMPU-6100A.pdf.

[5] A. Platit, J. Kubik, M. Vopalensky, and P. Ripka, "Precise AMR magnetometer for compass," in *Proc. IEEE Sensors*, Oct. 22–24, 2003, pp. 472–476.

[6] P. Haumer, H. Hauser, P. L. Fulmek, and D. Bajalan, "Hysteresis modeling of thin permalloy films and parameter interpretation," *IEEE Trans. Magn.*, vol. 40, no. 4, pp. 2745–2747, Jul. 2004.

[7] R. Ferreira, E. Paz, P. P. Freitas, J. Ribeiro, J. Germano, and L. Sousa, "2-Axis magnetometers based on full Wheatstone bridges incorporating magnetic tunnel junctions connected in series," *IEEE Trans. Magn.*, vol. 48, no. 11, pp. 4107–4110, Nov. 2012.

[8] R. Racz, C. Schott, and S. Huber, "Electronic compass sensor," in *Proc. IEEE Sensors*, Oct. 24–27, 2004, pp. 1446–1449.

[9] C. Schott, R. Racz, A. Manco, and N. Simonne, "CMOS single-chip electronic compass with microcontroller," *IEEE J. Solid-State Circuits*, vol. 42, no. 12, pp. 2923–2933, Dec. 2007.

[10] M. J. Thompson and D. A. Horsley, "Resonant MEMS magnetometer with capacitive read-out," *IEEE Sensors*, pp. 992–995, Oct. 25–28, 2009.

[11] J. Kyynarainen, J. Saarilahti, H. Kattelus, A. Karkkainen, T. Meinander, A. Oja, P. Pekko, H. Seppa, M. Suhonen, H. Kuisma, S. Ruotsalainen, and M. Tilli, "A 3D micromechanical compass," *Sens. Actuators A, Phys.*, vol. 142, no. 2, pp. 561–568, Apr. 2008.

[12] H. Emmerich and M. Schoefthaler, "Magnetic field measurements with a novel surface micromachined magnetic-field sensor," *IEEE Trans. Electron Devices*, vol. 47, no. 5, pp. 972–977, May 2000.

[13] M. J. Thompson, M. Li, and D. A. Horsley, "Low power 3-axis Lorentz force navigation magnetometer," in *Proc. IEEE Conf. MEMS*, Cancun, Mexico, Jan. 23–27, 2011, pp. 593–596.

[14] C. Buffa, G. Langfelder, A. Longoni, A. Frangi, and E. Lasalandra, "Compact MEMS magnetometers for inertial measurement units," *IEEE Sensors*, pp. 28–31, Oct. 2012.

[15] V. Kempe, "Gyroscopes," in *Inertial MEMS Principles and Practice*. Cambridge, U.K.: Cambridge Univ. Press, 2011, ch. 8.

[16] C. Acar, A. R. Schofield, A. A. Trusov, L. E. Costlow, and A. M. Shkel, "Environmentally robust MEMS vibratory gyroscopes for automotive applications," *IEEE Sensors J.*, vol. 9, no. 12, pp. 1895–1906, Dec. 2009.

[17] G. Langfelder, T. Frizzi, A. Longoni, A. Tocchio, D. Manelli, and E. Lasalandra, "Readout of MEMS capacitive sensors beyond the condition of pull-in instability," *Sens. Actuators A*, vol. 167, pp. 374–384.

[18] V. Kempe, "Non-inertial forces," in *Inertial MEMS Principles and Practice*. : Cambridge Univ. Press, 2011, ch. 3.

[19] C. T.-C. Nguyen and R. T. Howe, "CMOS micromechanical resonator oscillator," in *Proc. Electron Dev. Meeting Tech. Dig Int.*, Dec. 1993, pp. 199–202.

[20] *EQ-411L Hybrid Linear Hall Effect ICS*. Tokyo, Japan: Asahi Kasei Microdevices, 2009 [Online]. Available: https://www.asahi-kasei.co.jp/asahi/en/.

[21] R. N. Dean, S. T. Castro, G. T. Flowers, G. Roth, A. Ahmed, A. Scottedward Hodel, B. E. Grantham, D. A. Bittle, and J. P. Brunsch, "A characterization of the performance of a MEMS gyroscope in acoustically harsh environments," *IEEE Trans. Ind. Electron.*, vol. 58, no. 7, pp. 2591–2596, Jul. 2010.

[22] M. Lemkin and B. E. Boser, "A three-axis micromachined accelerometer with a CMOS position-sense interface and digital offset-trim electronics," *IEEE J. Solid-State Circuits*, vol. 34, no. 4, pp. 456–468, Apr. 1999.

[23] J. Wu, G. K. Fedder, and R. Carley, "A low-noise low-offset capacitive sensing amplifier for a $50\ \mu g/\sqrt{Hz}$ monolithic CMOS MEMS accelerometer," *IEEE J. Solid-State Circuits*, vol. 39, no. 5, pp. 722–790, May 2004.

[24] M. Paavola, M. Kämäräinen, E. Laulainen, M. Saukoski, L. Koskinen, M. Kosunen, and K. A. I. Halonen, "A micropower $\Delta\Sigma$-based interface ASIC for a capacitive 3-axis micro-accelerometer," *IEEE J. Solid-State Circuits*, vol. 44, no. 11, pp. 3193–3210, Nov. 2009.

[25] A. Frangi, A. Ghisi, and L. Coronato, "On a deterministic approach for the evaluation of gas damping in inertial MEMS in the free-molecule regime," *Sens. Actuators A, Phys.*, vol. 149, no. 1, pp. 21–28, Jan. 2009.

[26] M. Li, V. T. Rouf, M. J. Thompson, and D. A. Horsley, "Three-axis lorentz-force magnetic sensor for electronic compass applications," *J. Microelectromech. Syst.*, vol. 21, no. 4, pp. 1002–1010, Aug. 2012.

[27] A. L. Herrera-May, P. J. García-Ramírez, L. A. Aguilera-Cortés, E. Figueras, J. Martínez-Castillo, E. Manjarrez, A. Sauceda, L. García-González, and R. Juárez-Aguirre, "Mechanical design and characterization of a resonant magnetic field microsensor with linear response and high resolution," *Sens. Actuators A*, vol. 165, no. 2, pp. 399–409, Feb. 2011.

[28] F. Keplinger, S. Kvasnica, A. Jachimowicz, F. Kohl, J. Steurer, and H. Hauser, "Lorentz force based magnetic field sensor with optical readout," *Sens. Actuators A*, vol. 110, no. 1–3, pp. 112–118, Feb. 2004.